This is to certify that the

thesis entitled

The effect of Rolling on the Redistribution of SiC_p Clusters and its Influence on the Mechanical Properties of 10% SiC_p/6061-Al Composites

presented by

Jae-chul Lee

has been accepted towards fulfillment
of the requirements for

Master's of Science degree in Material Science

K. N. Subramanian.

Major professor

Date 7/25/89

THE EFFECT OF ROLLING ON THE REDISTRIBUTION OF SiC_p CLUSTERS AND ITS INFLUENCE ON THE MECHANICAL PROPERTIES OF 10 % SiC_p/6061-Al COMPOSITES

by Jae-Chul Lee

A THESIS

submitted to
Michigan State University
in partial fulfillment of the requirements
for the degree of

MASTER OF SCIENCE

Department of Metallurgy, Mechanics and Materials Science

1989

ABSTRACT

Warm rolling in a direction perpendicular to the direction of banding in SiC_p/6061 Al-alloy composites having a severely banded SiC_p clusters causes significant redistribution of SiC_p within the composites. The mechanical properties were found to become more isotropic with increased percent of reduction. The strength and elongation parallel to the rolling direction were found to increase with increasing reduction ratio up to 50-60%. On the other hand the properties perpendicular to the rolling direction were found to decrease slightly with increasing reduction ratio. Such phenomena are analyzed based on metallographic and fractrographic examinations.

Possible mechanisms operative in the strengthening of SiC_p/Al composites are considered. Failure mechanism of SiC_p/Al composites under uniaxial tension is proposed.

Acknowledgement

I would like to take this oppertunity to sincerely thank my advisor, Dr. K. N. Subramanian, for his constant support and guidance during the research. Without his encouragement and help this study would have been far from reality.

I would also like to thank Dr. A. Hingwe and R. Vaidya for supporting me the material used for the research.

I would like to take this opportunity to extend my most sincere gratitude to my parents, brother, and sister for their sacrifice. Last but not the least, a special thanks to my wife, Chae-Hong, for her endurance and assistance.

TABLE OF CONTENTS

LIST OF FIGURES

LIST OF TABLES

1. INTRODUCTION

Since the early 1960s, with the impetus of high temperature structural applications, various kinds of metal matrix composites have been investigated by incorporating high strengh ceramic materials such as alumina(Al_2O_3) and silcon carbide(SiC) whiskers, and boron carbide(B_4C) particulates into molten metals [1,2].

Among many of those metal matrix composites, continuous graphite fiber/copper, continuous graphite fiber/aluminum alloy, SiC(whisker and particulate)/aluminum alloy, Al_2O_3(particulate)/ magnesium, SiC(particulate)/magnesium were particularly promising for structural applications. But the cost of ceramic renforcements prevent the composites from the practical applications inspite of their attractive mechanical properties to the engineers and designers.

In 1973, as the new technology for making β-SiC whisker by pyrolizing rice hull was developed, silicon carbide whiskers could be made much cheaper, finer, and purer than previous ones.

Since then, especially during the past ten years, silicon carbide reinforced aluminum matrix composites have been studied extensively in many areas, due to their potentials in automotive, structural, and aeronautical applications.

Many of these studies carried out so far deal with continuous fiber and discontinuous whisker reinforced composites. Although these composites are as light as aluminum and its alloys, they possess a significant improvement in strength and stiffness [3-9], fatigue resistance [10-12], damping capacity [13],and wear resistance [14,15], in addition to high temperature properties [15-17]. Particularly, strength and stiffness of SiC particulate reinforced Al-alloy matrix composites (SiC_p/Al composites) are comparable to titanium and its alloys [18,19], and enable them to replace titanium forgings. For example, the ultimate tensile strength and the stiffness of silicon carbide fiber reinforced aluminum matrix composites are much higher than those of unreinforced titanium even at 500^{o}C [19].

However, the main drawback of these continuously reinforced composites are their severe anisotropy in mechanical properties. In addition, it is difficult to fabricate, and shape them into their final configurations. On the other hand, SiC_p/Al composites can be manufactured relatively easily and economically by melting and casting techniques. For example, near-net shapes of track shoes and pistons can be produced by using squeeze casting method [20]. The basic principle of the squeeze casting is to 'forge' a liquid metal into a closed die to reduce the porosity due to the shrinkage and gas, and to make the products solidify rapidly under high pressure of 50 to 100

MPa. In order to significantly increase the volume fraction of reinforcement without flocculation, Rheocasting (compocasting), which consists of vigorously agitating a semisolid composites before casting [21] can be effectively used.

Moreover, unlike polymer matrix composites and discontinuous fiber reinforced composites, which are usually formed into the final shapes, metal matrix composites containing particulate reinforcements can be shaped into their final configurations by using the conventional mechanical workings such as forging, extrusion, and rolling, etc. Such components as automobile-engine connecting rod and compressor blade can be forged from bar stock that was extruded from a cast billet [22].

Such mechanical workings to obtain the final shape will alter the size, shape, and distribution of clustered particulates. All these parameters have significant influences on the mechanical properties of such a composite system.

Recently, it has been found that nearly all commercially important ceramic reinforcements including silicon carbide have a poor wettability by molten aluminium and its alloys [23-25]. As a result of the poor wettability of silicon carbide by molten matrix alloys, the direct incorporation of SiC_p into molten aluminum alloys causes flocculation. Under such conditions, extensive clustering or

agglomeration of the particulates occurs in order to reduce surface tension. This effect becomes more significant as the particulate size becomes smaller than 40 μm [27,28] and the difference in density between the matrix alloy and reinforcements becomes larger [15].

Such clustering not only cause poor overall mechanical properties and machinability [28], but also cause anisotropy of particulate reinforced composites in their as-manufactured state and prohibit the wider use of these composites for practical applications. If the distribution of the SiC_p can be made more uniform, the properties of these composites can become more isotropic.

A number of different techniques have been used to overcome this problem. The following methods have been found to be very effective in preventing significant particulate clusterings or agglomerations.

1) **Matrix modification** by adding some alloying elements, such as Li or Mg, has been proved to be effective in improving the wettability of the reinforcements by the molten matrix [14,27,29-32]. These alloying additives are added just before incorporating the reinforcements into molten matrix.

2) **Preheating** the reinforcements before introducing into molten matrix allows their uniform distribution in the matrix [31,33].

3) The use of **particulate coatings**, such as Ni or Cu coatings on graphite or alumina particles, has been tried

out successfully and thereby improves the wettability by the molten aluminum alloys [34].

Mechanical working of the composites can be used as another means for making the SiC_p to be uniformly distributed. Rolling has been used very effectively in hypoeutectoid steels to break up pearlite lamella and to obtain a semi-spherodized struture. The principle behind this process is the differece in the ductilities of the ferrite and pearlite. During rolling, the pearlite phase tends to break up due to its lower ductility. The SiC_p/Al composites are very similar to hypoeutectoid steels in this point of view. The aluminum matrix has much higher ductility as compared to the brittle SiC_p clusters. Hence, it is expected that rolling can break up the clusters of the SiC_p and thereby change the mechanical properties of the composite system.

Very few investigations have studied the effects of mechanical working on the composites so far [6,18,35,37]. However, various investigations have been focussed on the charecterization of the interface [37-40], mechanical properties at room and elevated temperatures, and on various manufacturing processes.

The objectives of the present study are

1) to investigate the effects of warming rolling on the size and distribution of the SiC_p clusters and its influence on the mechanical properties

2) to evaluate the variation in the mechanical properties of the SiC_p/Al composites after different amounts of deformations and heat treatments.

3) to identify the strengthening mechanisms operative in SiC_p/Al composites

4) to propose a failure mechanism of SiC_p/Al composites under uniaxial tension.

2. STRENGTHENING MECHANISM OF SiC_p/Al COMPOSITES

The addition of ceramic reinforcement in the forms of fibers, whiskers, and particulates into metal matrix can lead to significant increases in yield strength and elastic modulus as compared to those of the matrix, while there are some negative effects on the mechanical properties such as decreases in ductility and fracture toughness.

Although the theories for the strengthening mechanism of the SiC_p/Al composites have not yet been completely estabilished, some plausible strengthening mechanisms, such as Orowan theory, composite strengthening from modified shear lag theory, thermal strain hardening due to enhanced dislocation density, and strengthening due to smaller subgrain and grain, can be used to explain the strengthening of discontinuously reinforced SiC/Al composites.

Therefore the expected yield strength of the SiC_p/Al composites can be expressed as

$$\sigma_{cy} = \sigma_{my} + \Delta\sigma \qquad \text{--------- 1)}$$

where σ_{cy} = yield strength of the composites

σ_{my} = yield strength of the matrix

$\Delta\sigma$ = increased amount in yield strength

$= \Delta\sigma_{orowan} + \Delta\sigma_{comp} + \Delta\sigma_{disloc} + \Delta\sigma_{sub\ gr.}$

$\Delta\sigma_{orowan}$ = increased amount in yield strength due to dislocation looping

$\Delta\sigma_{disloc}$ = increased amount in yield strength due to the enhanced dislocation density

$\Delta\sigma_{sub\ gr.}$ = increased amount in yield strength due to the formation of subgrain

$\Delta\sigma_{comp}$ = increased amount in yield strength due to load transfer

The principle idea for calculating $\Delta\sigma_{comp}$ is the application of the continnum mechanics to the composite strengthening. The externally applied load is transferred from the matrix (Al alloy) to the reinforcement (SiC_p) via the SiC_p/Al interface. The strengthening depends on the interfacial bonding strength and the efficiency of the load transfer from the matrix to the reinforcement i.e, shape of the reinforcement.

The material properties used in this thesis are listed in Table.1.

Material \ Property		Y.S (MPa)	UTS (MPa)	ϵ_f (%)	E (GPa)	ν	α $(mm \cdot {}^{\circ}K)^{-1}$	Ref
6061Al	TO	55	124	25 - 30	68.3	0.33	28×10^{-6}	41
	T6	235	267.5	12	74	0.33	28×10^{-6}	41
SiC		1380	–	–	438	0.19	3×10^{-6}	42

Table 1. Slected properties of the 6061-Al and SiC used in this thesis

Note : 1. T6 : Solution treatment : $529^{\circ}C$ * 70 min.
R.T. aging : $24^{\circ}C$ * 48 hours
Artificial aging : $200^{\circ}C$ * 10 hours

2. ϵ_f : Fracture elongation

3. E : Elastic modulus

4. ν : Poisson's ratio

5. α : Thermal expansion coefficient

2.1 Orowan strengthening

Since most of the SiC exists in the form of particles, it may be possible to propose the Orowan strengthening mechanism. The Orowan-Ashby equation [43] or looping of precipitates is given by

$$\Delta\tau = [0.81 \cdot \mu \cdot b]/[2\pi \cdot (1-\nu)^2 \cdot D^2] \cdot \ln(2r_0/b) \quad \text{---- 2)}$$

where $\Delta\tau$ = increased amount in resolved shear stress due to the precipitates

μ = shear modulus of the matrix (28 GPa for 6061 Al -T6 treated

ν = Poisson's ratio (0.33)

r_0 = mean particulate radius

b = Burger's vector ($2.86*10^{-8}$cm)

D = effective interparticulate spacing [44]

$= (Lt/V_p)^{1/2}$

L = length of particulate

t = thickness of particulate

V_p = volume fraction of the particulate

Generally, the increased amounts in yield strength ($\Delta\sigma$) is expressed as

$$\Delta\sigma = M \cdot \Delta\tau \quad \text{------- 3)}$$

where M is approximately 2.

The evaluated increases in yield strength ($\Delta\sigma$) is only about 2 MPa, while the observed increases in yield-strength for T6 tempered composites is 67 MPa.

It is obvious from eq-2) that the amount of the strengthening due to the Orowan mechanism is strongly dependent on the interparticulate spacing. However, the interparticulate spacing between the SiC_p in the composites is usually too large for dislocations to be bowed between the SiC_p during deformation. Hence, in this point of view, it is considered that the Orowan strengthening mechanism contributes very little to the strengthening of the SiC_p/Al composites.

2.2 Composite Strengthening

In 1952, Cox developed the shear lag model to predict the yield strength of short fiber reinforced composites [45]. The most important assumption in the shear lag model is that the load transfer occurs only between the fiber and matrix by means of shear sterss at the fiber-matrix interface. This theory can be used successfully for predicting the yield strength of composites having large aspect ratio reinforcement.

However, underestimation in yield strength are expected for the composites having small aspect ratio such as whisker or particulate reinforced composites, because the normal load transfer at the whisker and particulate ends and side surfaces was ignored in the shear lag theory.

In 1986, Nardone and Prewo proposed a modified shear lag model to explain the strengthening of discontinuously reinforced composites having small aspect ratio reinforcements such as SiC_p and SiC_w [46]. Although this theory took into account of the normal load transfer at the whisker and particulate ends, the normal load transfer at the side surfaces of the whisker and particulate was still ignored.

The modified shear lag theory for particulate reinforced composites gives the composites yield strength (σ_y) by the following equation[46]:

$$\sigma_y = \sigma_{my} \cdot [1 + (L_1+t) \cdot s/4L_1] \cdot V_p + \sigma_{my} \cdot V_m \quad \text{------- 4)}$$

where σ_{my} = yield strength of the matrix
= 235 MPa for 6061 Al-T6

L_1 = length of the particulate perpendicular to the applied stress

t = thickness of the particulate

V_p = volume fraction of the SiC_p

V_m = volume fraction of the matrix
= $1 - V_p$

s = particulate shape factor = $2L/t$

L = particulate length in the tensile direction.

Assuming $L_1 \approx t$ gives

$$\sigma_y = \sigma_{my} \cdot [1 + s/2] \cdot V_p + \sigma_{my} \cdot V_m. \quad \text{--------- 5)}$$

Therefore, the increases in yield strength due to load transfer ($\Delta\sigma_{comp}$) is

$$\Delta\sigma_{comp} = \sigma_y - \sigma_{my}$$
$$= \sigma_{my} \cdot [(1+s/2) \cdot V_p + V_m - 1]$$
$$= \sigma_{my} \cdot (s/2) \cdot V_p . \quad \text{--------- 6)}$$

According to Eq-6), once the particulate shape factor s is fixed, the increases in composite yield strength $\Delta\sigma_{comp}$ depends only on the volume fraction of reinforcement or vice versa. Moreover, $\Delta\sigma_{comp}$ has no relationship with the

strength of the reinforcement. Appropriate values of s(=3) and V_p(=0.1) give $\Delta\sigma_{comp}$ = 35.3 MPa.

On the other hand, $\Delta\sigma_{comp}$ can also be expressed in terms of interparticulate spacing (D) by the following procedure:

s = particulate shape factor

$$= 2L/t \qquad \text{---------- 7)}$$

D = effective interparticulate spacing

$$= \sqrt{(L \cdot t/V_p)} \qquad \text{---------- 8)}$$

Solving eq-7) and eq-8) for 's' gives

$$s = (2D^2 V_p)/t^2 \ . \qquad \text{---------- 9)}$$

Substitutinon of eq-9) into eq-6) gives the relationship between $\Delta\sigma_{comp}$ and interparticulate spacing (D)

$$\Delta\sigma_{comp} = \sigma_{my} \cdot (V_p/t)^2 \cdot D^2 \qquad \text{---------- 10)}$$

Therefore, for a fixed volume fraction of the reinforcement, if the average size of the reinforcement becomes finer, the interparticulate spacing will decrease by eq-8), thereby the composites yield strength is expected to increase substantially.

2.3 Thermal strain hardening

Arsenault and Fisher proposed a strengthening mechanism which can be explained by an enhanced dislocation density which is caused by the large difference (10:1) in the thermal expansion coefficient between the Al matrix and SiC_p in the composites [47]. A high dislocation density of 10^{9}-10^{12} cm^{-2} was observed experimentally during cooling down from the annealing temperature to the room temperature [48]. The increase in the shear stress($\Delta\tau$) due to the presence of dislocations can be expressed as

$$\Delta\tau = \alpha' \cdot \mu \cdot b \cdot \sqrt{\rho} \qquad \text{---------- 11)}$$

where $\alpha' \approx 0.5$

μ = shear modulus of matrix (28 GPa for 6061 Al-T6)

b = Burger's vector ($2.86*10^{-8}$ cm)

ρ = dislocation density of the matrix

Therefore, the following equation may be used for estimating the increase in yield strength ($\Delta\sigma_{disloc}$) due to the enhanced dislocation density:

$$\Delta\sigma_{dislo} = \alpha \cdot \mu \cdot b \cdot (\sqrt{\rho} - \sqrt{\rho_o}) \qquad \text{---------- 12)}$$

where α = 1.25 for Al [49]

ρ = dislocation density of the matrix of the SiC_p/Al composites

ρ_0 = dislocation density of the matrix in the absence of SiC_p ($\approx 10^{-6} cm^{-2}$ for annealed Al).

Since ρ is much bigger than ρ_0, eq-12) can be reduced into

$$\Delta\sigma_{disloc} = \alpha \cdot \mu \cdot b \cdot \sqrt{\rho}$$
$$= 1.25\mu \cdot b \cdot \sqrt{\rho} \ . \qquad \text{---------- 13)}$$

In 1986, Arsenault and Shi developed an equation for evaluating the dislocation density by using the model of "the prismatic punching of dislocations" [50]. From their analysis, the dislocation density in the matrix was found to be

$$\rho = [B \cdot V_p \cdot \Delta\epsilon]/[(1-V_p) \cdot b \cdot d] \qquad \text{---------- 14)}$$

where B = a geometric constant between 4 and 12
= 8 (for particulate reinforcement)

V_p = volume fraction of reinforcement

$\Delta\epsilon$ = misfit strain due to the difference in the thermal expansion coefficient
$= \Delta\alpha \cdot \Delta T$

b = Burger's vector

d = the smallest dimension of the particulate

Substitution of eq-14) into eq-13) results in the final expression for the increases in yield strength due to the enhanced dislocation density.

$$\Delta\sigma_{disloc} = 3.54\mu \cdot b \cdot [\ (V_p \cdot \Delta\alpha \cdot \Delta T)/\{(1-V_p) \cdot b \cdot d\}\ ] \quad .\text{-- 15)}$$

For a fixed volume fraction of reinforcement, from eq-15) it is expected that $\Delta\sigma_{disloc}$ will increase significantly by incorporating the smaller size of reinforcement. For V_p=0.1 and d=10μm, at least a 22 MPa increase in yield strength is expected due to the enhanced dislocation density.

2.4 Strengthening due to subgrain

A smaller grain and subgrain size as compared to those of the wrought Al alloy can also lead to a significant increase in yield strength.

Since the interface between SiC and Al matrix act as a source of dislocation generation, small subgrains are expected to be formed near SiC_p due to tangling of dislocations. Arsenault and Fisher observed a high dislocation density of 10^{10} cm^{-2} and small subgrains of 1.5-2.5 μm in size in an SiC/Al composites during cooling from annealing temperature in an in situ experiment with a transmission electron microscopy (TEM) [47]. On the other hand, the fracture surface of the wrought Al alloy reveals relatively large subgrain of 5 μm in size [48,50]. Such results can also be verified by examining a fracture surface of the composites with a scanning electron microscopy (SEM), since the dimple size almost corresponds to the subgrain size [48,51]. Fig.1) shows the dimple sizes of the reinforced and the unreinforced Al alloy. $\Delta\sigma_{sub\ gr.}$ is equal to 29.4 MPa for an average subgrain size of 2.5 μm observed in Fig.2).

The Hall-Petch relation can be a possible candidater for the strengthening of SiC_p/Al composites, because the incorporation of SiC_p into the molten Al alloy and the rapid solidification of the composite system obstruct grain growth during cooling from fabrication temperature.

Figure 1. Fractographs showing the dimple size in

a) unreinforced aluminium alloy
b) aluminium alloy reinforced with 10 % SiC_p

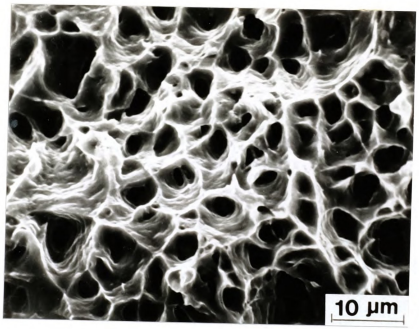

a)

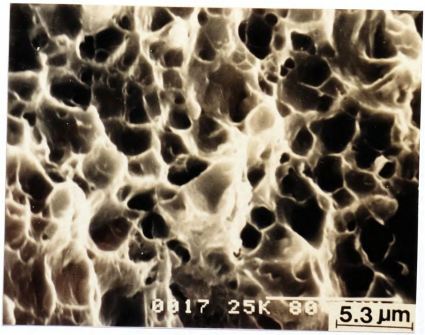

b)

Figure.1

Figure 2. The correlation between steady flow stress and mean subgrain diameter of commercial aluminium for various deformation conditions

● : Compression [52]
□ : Extrusion [53]
△ : Creep [54]
⬡ : Hot torsion [55]

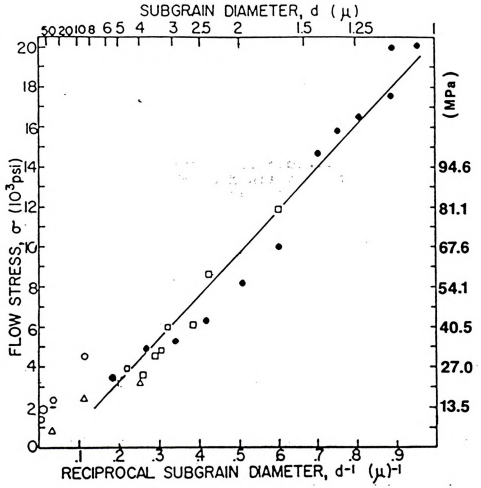
SUBGRAIN DIAMETER, d (μ)
50 20 10 8 6.5 4 3 2.5 2 1.5 1.25 1
FLOW STRESS, σ (10³psi)
(MPa)
94.6
81.1
67.6
54.1
40.5
27.0
13.5
RECIPROCAL SUBGRAIN DIAMETER, d⁻¹ (μ)⁻¹

Figure.2

The grain sizes between the reinforced and the unreinforced Al alloy are compared in Fig.3).

Therefore, due to above considerations, at least 89 MPa of theoretical increases in yield strength is expected with the incorporation of 10% SiC_p. This gives the lower bound value for a theoretical yield strength of 324 MPa without including the strengthening due to small grain size (Hall-Petch relation). However, the measured yield strength of the 10%-SiC_p/6061-Al composites was only 302 MPa in their longitudinal direction.

The mismatch between the theoretical and measured yield strength seemed to be due to the following factors :

1) Random orientation of some of the SiC_p with respect to the tensile direction
2) Pre-existing porosity (or void) in the matrix
3) Pre-existing debonding at the interface
4) Particulate free-zone that may results in big sub-grain
5) Particulate cracking from fabrication i.e during extrusion process

Figure 3. Metallograph illustrating the grain size of

a) unreinforced aluminium alloy
b) aluminium alloy reinforced with 10 % SiC_p

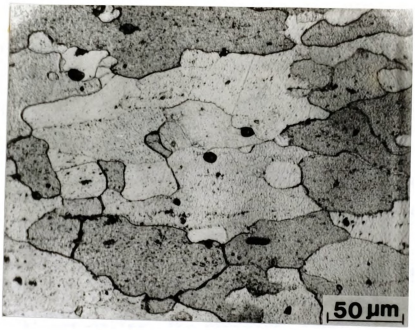

a)

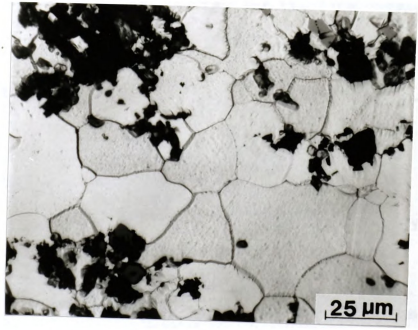

b)

Figure.3

3. EXPERIMENTAL PROCEDURE

3.1 Material

6061 aluminium alloy reinforced with 10 % (by volume) of SiC_p, procured as an extruded cylinderical bar of diameter 64.3 mm from ALCAN, was used for this study. The matrix of the composites was characterized by using EDAX after solutionizing.

The line intercept method and the grid analysis [56] were used to determine the volume fraction of the SiC_p in the SiC_p/Al composites. The schematic drawings illustrating these methods are shown in Fig.4-a) and Fig.4-b). The following relation was assumed for the line intercept method and the grid analysis [57].

$$V_f = \langle A_f \rangle = \langle L_f \rangle = \langle P_f \rangle \qquad \text{---------- 16)}$$

where V_f = volume fraction of SiC_p

$\langle A_f \rangle$ = average area fraction

= ratio of the area which is covered by SiC_p to the total area tested

$\langle L_f \rangle$ = average line fraction

= ratio of the length of the line which is intercepted by SiC_p to the total length of the test line

Figure 4. a) Grid analysis
b) Line intercept method

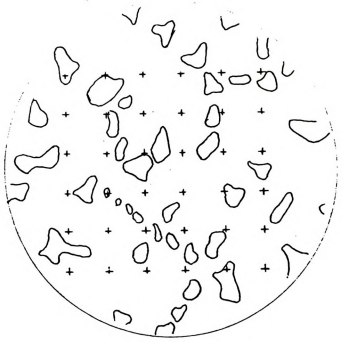

a)

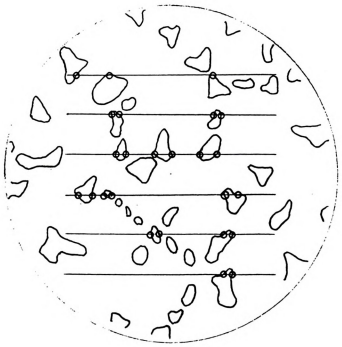

b)

Figure.4

$\langle P_f \rangle$ = average point fraction

= ratio of the number of points which lie in the SiC_p to the total number of points in the grid.

In order to investigate the effect of warm rolling on the distribution of SiC_p, the composites with a severely banded structure of SiC_p clusters in the direction of extrusion were used for the tests. A three dimentional view of the as-extruded composites is shown in fig.5). The amount of the pre-existing porosity (Fig-6) was determined as 1-2 % from the grid analysis.

The average particulate size was found to be 10 μm with the help of the line intercept method.

$$d = L/(n.M) \qquad \text{--------- 17)}$$

where d = the average particulate size

L = the length of the test line

n = the number of intersections with SiC_p and test line which is drawn in the micrograph concerned, and

M = the magnification.

Figure 5. Three dimentional view of as-extruded 10 % SiC_p/6061-Al composite

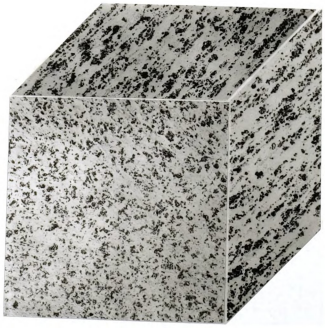

Figure.5

Figure 6. Porosities of the as-extruded SiC_p/Al composite viewed parallel to the extrusion direction

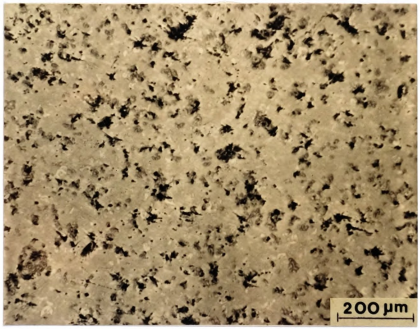

Figure.6

3.2 Specimen Preparation

The stock material was cut out from a cylindrical bar which was obtained in the as-extruded (as-manufactured) state, and rolled unidirectionally into different percentages of reduction in a direction perpendicular to the extruded direction, namely, transverse direction.

The reduction ratio (R) can be defined as the reduction in thickness from the assumption of plane strain condition.

$$R = [\ (\ A_o - A_f\ )/A_o\ ] \times 100\ [\%]$$
$$= [\ (\ t_o - t_f\ )/t_o\ ] \times 100\ [\%] \qquad \text{--------- 18)}$$

where A_o = initial cross sectional area of the specimen
A_f = final cross sectional area of the specimen
t_o = initial thickness of the specimen, and
t_f = final thickness of the specimen.

In order to maximize matrix flow and therefore minimize the particulate cracking and the possible interface debonding, warm rolling was carried out at a temperature below 400°C. At the same time, a high reduction ratio, but less than 10% of reduction per each pass, was used to get homogeneous matrix flow, which was found to be effective in separating the SiC_p clusters into separate particulates.

After each pass of rolling, the specimens were annealed for 5- 7 min. at 415°C in order to get rid of the

dislocations which were induced due to rolling process. This was checked by measuring the hardness, i.e, regardless of the reduction ratio the value of HR_B20 was obtained after annealing.

The rolled sheets which were reduced by different percentages of reduction, were cut into parallel (longitudinal) and perpendicular (transverse) to the extruded directions with a diamond sawing machine. The schematic drawing is shown in Fig.7).

The sheet tensile specimens were made by hands with files. The specimens were polished with abrasive papers and rotating laps in order to remove the contact surface with rolls during rolling process. The final shape and dimensions of the tensile specimen is shown in Fig.8).

Two kinds of heat treatments were used before testing the specimens, i.e, full annealing (T0) and artificial aging (T6). Especially for the full annealed specimen, the test was carried out within 30 min in order to prevent the precipitation from the matrix even at room temperature. Yhe heat treatment conditions used can be described as following:

1) Full annealing (T0 temper)
   -In order to get the softest codition, the specimens were heated at 415^{0}C for 2 hours then quenched into cold water.
2) Artificial aging (T6 Temper)

-solution treatment : 530°C for 70 min.
(cold water quenching)
-room temperature aging : 24°C for 48 hours
-artificial aging : 200°C for 10 hours

Figure 7. a) Section of the extruded bar stock cut out for specimen preparation

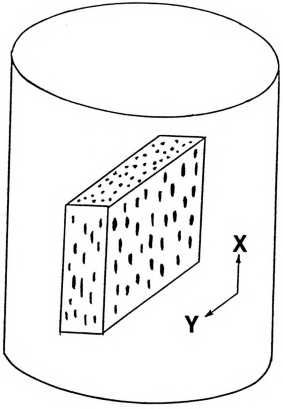

X = Extrusion direction
= (Longitional direction)

Y = Rolling direction
= (Transverse direction)

Figure.7-a)

Figure 7. b) Schematic of procedure used for making specimens

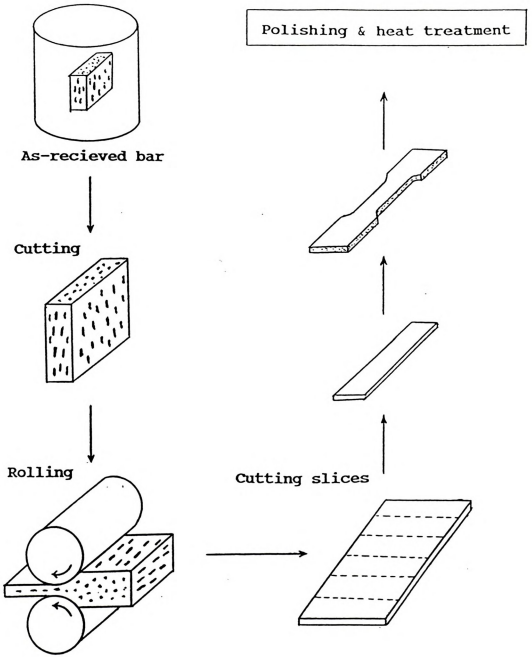
Polishing & heat treatment
As-recieved bar
Cutting
Rolling
Cutting slices

Figure.7-b)

Figure 8. Dimensions of sheet tensile specimen

W = Width of the specimen (5 mm)
L = Gauge length (17 mm)
T = THickness (0.7 mm)

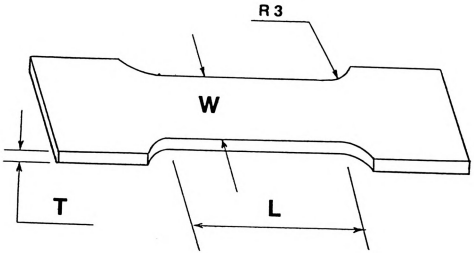

Figure.8

3.3 Tensile Test

The basic mechanical properties after various treatments of the specimen were measured using an Instron machine operated at a constant crosshead speed of 0.1 cm/min. The tests were carried out in a laboratory air enviornment at room temperature.

In order to prevent the slipping of the specimen from the grip, slices of file with small grooves were attached to the grips as in Fig.9).

Figure 9. Details of the grips

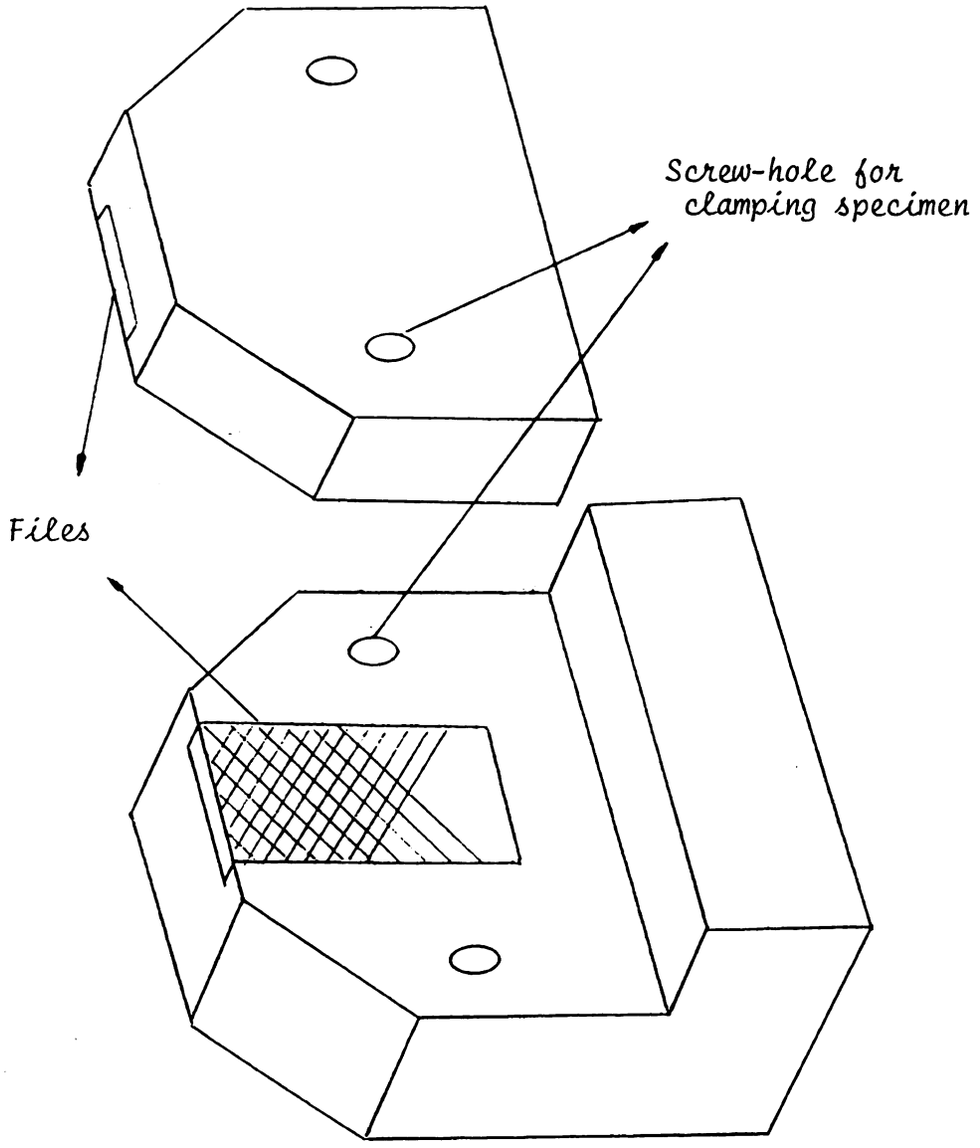

Figure.9

3.4 Fractographic and Metallographic Examination

The fracture surface of tensile specimens were examined by scanning electron microscope (SEM). In addition, metallographically polished surface of a mounted specimen was prepared to examine the cracking of SiC_p which can be caused due to compressive and tensile force.

The redistribution of SiC_p clusters due to rolling were examined with optical microscope.

The standard method of surface preparation consisted of successive surface removal by 240, 400, and 600 grit SiC abrasive paper, first and second polishing on rotating laps with 5 μm and 1 μm alumina powder, and finally first and second stage polishing on rotating laps with 1 μm and 0.25 μm diamond powders.

The Kellers Reagant was used for slight etching. Dilute HCl was used for deep etching of specimen surface.

4. RESULTS AND DISCUSSION

4.1 Microstructural Features

One of the advantages of the discontinuously reinforced metal matrix composites is their formability into the net shapes by conventional mechanical working or by plastic deformation methods.

Both cold and warm rolling were attempted on as-extruded (as-received status) composites along a direction perpendicular to the extrusion direction, until edge cracks were observed on the specimens. Although controlled **cold rolling** was carried out (i.e 1-2 % reduction in thickness per each pass), edge cracks and surface scuffings were formed before 40 % reduction was reached. Such edge cracks and surface scuffings appeared to be formed mainly due to the large clusters of SiC_p which usually have micro-voids inside the clusters. The initiation and propagation of the edge cracks resulting from cold rolling can be observed in Fig.10). Once these cracks are formed, they tend to connect the SiC_p clusters and grow larger. Some of the cracks were observed to propagate along the broken SiC_p and the initially debonded interfaces as in Fig.11).

During cold rolling, the hardness of the composites increases very rapidly. For example, 30 % of reduction gives rise to an increase in hardness from HR_B20 (T0

Figure 10. Micrograph illustrating the initiation (X) and propagation (Y) of edge cracks along the clustered masses of SiC_p during rolling process

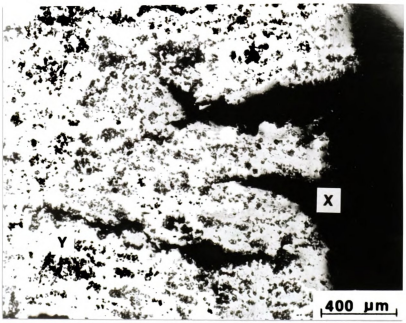

Figure.10

Figure 11. Micrographs illustrating the crack propagation along the cracked particles (a) and debonded interfaces (b) during rolling process

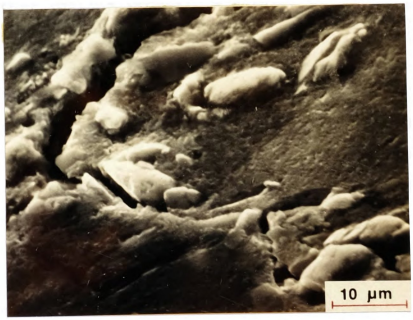

a)

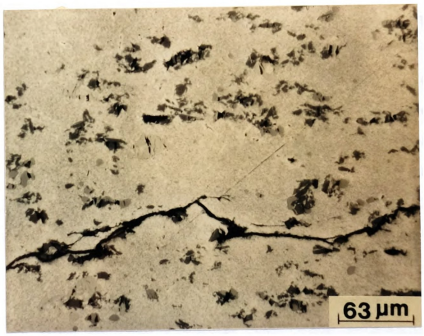

b)

Figure.11

tempered state) to HR_B55. Such an increase in hardness makes further rolling impossible without an additional stress relief annealing.

The rolled sheets of SiC_p/Al composites were cut parallel to the rolling direction, and examined metallographically on the polished sections. Significant particulate crackings were observed from the polished sections of the cold rolled SiC_p/Al composites. There is strong tendency for the crack planes to be parallel to the direction of compression (i.e rolling pressure) and to be perpendicular to the rolling direction(i.e feed direction). At the same time, it was found that the average size of the SiC_p that breaks is generally larger than the average size of all SiC_p in the composites. Such observations correspond to the results of Gurland [58] who had studied the fracture of cementite particles in a spherodized 1.05 % carbon steel, deformed under various loading conditions. He observed that the cementite particles, that cracked under uniaxial compression, were bigger than the average particle size, and that the particle cracking occuredalong a direction parallel to the compressive force. Such formations of particulate cracking can cause decrease in strength and ductility of the composites. The substantial increase in rolling pressure during cold rolling, as compared to that of warm rolling, was found to be responsible for such crackings of the SiC_pin the composites. This comparison is shown in Fig.12).

On the other hand, in case of **warm rolling**, the specimen could be rolled down to as much as 85 % of reduction without any edge crackings or surface scuffings. Although relatively large reduction ratio per each pass of rolling (about 6-7 %) was used, the first edge cracks made their appearence at about 85 % reduction. The results indicate that SiC_p/Al composites possess an excellent warm formability. Another advantage of warm rolling is that particulate crackings and interface debondings can be minimized (Fig.12), since the flow stress decreases monotonically with increasing temperature for both the reinforced and unreinforced material [36].

Both cold and warm rolling were found to cause a significant change in the distribution and shape of the SiC_p clusters. The most apparent difference in metallographic features between the as-extruded and the rolled composites is the presence of banded structure of SiC_p clusters. The microstructural features of the as-extruded and the warmed rolled composites with different reduction ratios are shown in Fig.13).

There appear to be no significant differences in the microstructural features of the distribution of SiC_p clusters between the cold and the warm rolled composites; however, it is evident from Fig.14) and Fig.15) that the cold rolled specimens exhibited the presence of larger voids and debonded interfaces as compared to the warm rolled specimens at the same reduction ratio (Fig.14).

Figure 12. a) Particulate cracking in 40 % cold rolled composite
b) Abscence of particulate cracking in 60 % warm rolled composite

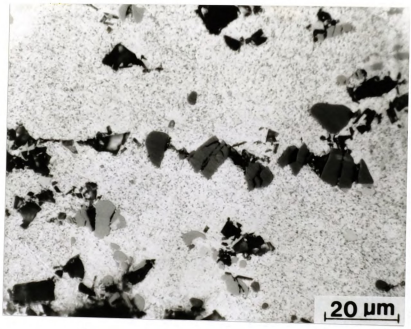

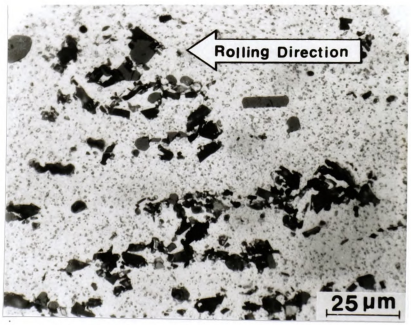

Figure.12

Figure 13. Micrograph exhibiting

a) the severely banded SiC_p clusters of as-received composite

b) the redistribution of SiC_p clusters in 40 % warm rolled composite

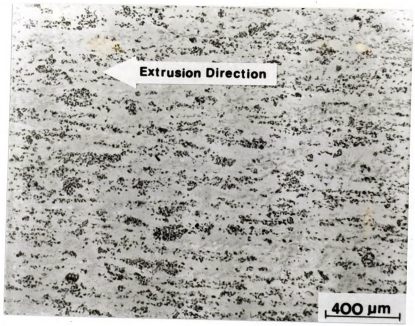

a)

b)

Figure.13

Figure 13. (continued)

Micrographs exhibiting the redistribution of SiC_p clusters in

c) 50 % warm rolled composite
d) 60 % warm rolled composite

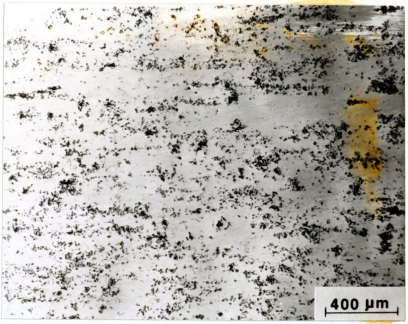

c

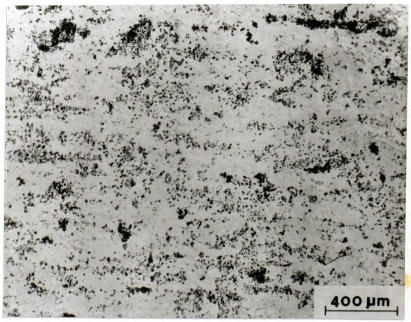

d

Figure.13 (continued)

Figure 13. (continued)

Micrograph exhibiting the redistribution of SiC_p clusters in

e) 70 % warm rolled composite

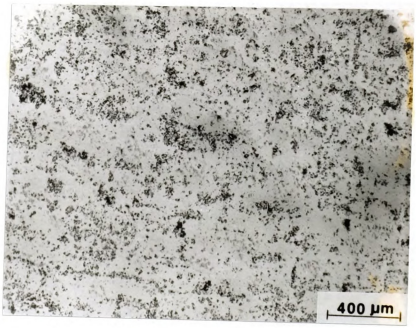

e

Figure.13 (continued)

Figure 14. Growth of pores during cold rolling

a) 70 % warm rolled
b) 70 % cold rolled

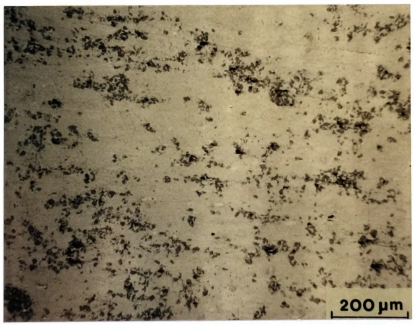

a

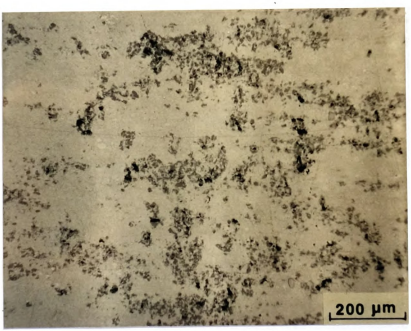

b

Figure.14

Figure 15. The comparision of the pores size between

a) as-received, and
b) 70 % warmed roled composite

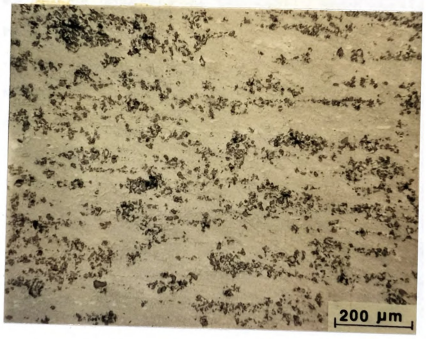

Figure.15

Moreover, these voids grow larger with increasing reduction ratio, as can be observer in Fig.15). Such features can b explained on the basis of enhanced plastic flow during warm rolling.

Hence, in order to facilitate matrix flow and to minimize either fracture of the SiC_p or debonding at the interface, plastic forming at higher temperature is recommended. Nevertheless, particulate cracking and interface debonding are observed even in the as-extruded SiC_p/Al composites, although they are not significant as compared to those formed during cold working process.

4.2 Mechanical properties

Some mechanical properties of the SiC_p/Al composites in their longitudinal and transverse directions, were measured at room temperature in the as-received and the warmed rolled status, both after T0 and T6 heat treatments.

Significant changes in mechanical properties compared with those of unreinforced Al-alloy, were observed for the 6061-Al alloy reinforced with 10 % of SiC_p. For example, compared with the wrought alloy, the SiC_p/Al composites revealed higher yield and ultimate strength, but lower fracture elongation. Also, compared with the T0 tempered SiC_p/Al composites, the T6 tempered SiC_p/Al composites were much higher in yield and ultimate strength but substantially lower in fracture elongation.

From the tensile testing of the SiC_p/Al composites in the longitudinal and transverse directions, it was observed that as-extruded composites exibited anisotropic mechanical properties, such as yield strength, ultimate strength, and fracture elongation, with respect to their longitudinal and transverse directions. It can be surmized from the Fig.10) that the microstructural inhomogeneity of the as-extruded composites may attribute to such anisotropic mechanical properties. On the contrary, the microstructure of the warm rolled composites becomes much more uniform (homogeneous) with increasing reduction ratio, which may result in more isotropic mechanical properties.

During tensile testing of the T0 tempered SiC_p/6061-Al composites with a cross-head speed of 0.1 cm/min, a strong dynamic strain hardening was observed just beyond the yield point of the composites. The interaction between the impurity atoms and the dislocations is reported to cause such an aging phenomenon during deformation [59]. It is also reported that dynamic strain aging tends to occur over a wide range of temperature,which depends on the strain rate [60]. The typical plot of load vs. elongation obtained with the Instron testing machine is shown in Fig.16). However, such strain aging phenomenon did not occur in T6 tempered composites, since oversaturated solute atoms are precipitated out during artificial aging procedure (T6) at 200^{0}C for 10 hours.

Although a significant redistribution of the SiC_p clusters was achieved with increasing reduction ratio of warm rolling, the principal effects of the warm rolling on the mechanical properties are to decrease the yield and tensile strength as well as the fracture elongation in the longitudinal direction. Some mechanical properties obtained at room temperature are presented in Tables 2, 3, and 4.

From the tables, it is evident that the as-extruded (as-received) composites have the largest ductility but the lowest strength, and the T6 tempered composites have the highest strength but the lowest ductility.

Figure 16. Load-elongation plot exhibiting dynamic strain aging behavior

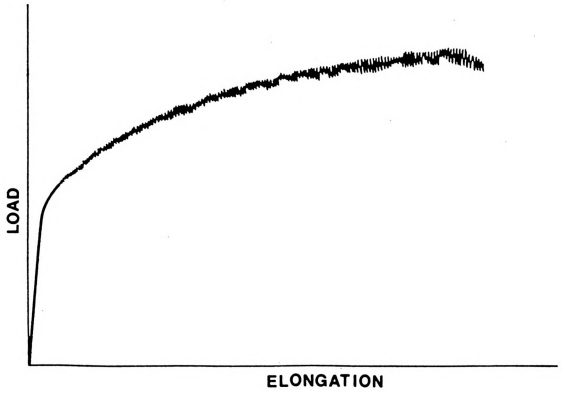

Figure.16

Specimen / R(%)	T O		T 6	
	L	T	L	T
0	124.2	115.7	302.0	269.5
20	-	-	-	-
30	-	-	288.7	281.6
40	-	-	-	-
50	119.3	119.0	285.1	282.1
60	119.1	119.0	283.2	283.0

Table 2. Variation in yield strength (in MPa) with respect to the reduction ratio along the transverse and the longitudinal directions

Specimen / R (%)	T O		T 6	
	L	T	L	T
0	231.1	201.2	368.6	323.0
20	-	-	-	-
30	-	-	356.2	339.6
40	-	-	-	-
50	222.2	222.4	351.5	342.0
60	220.6	222.1	350.0	347.2
70	214.3	207.0	-	-
80	209.0	207.0	-	-

Table 3. Variation in tensile strength (in MPa) with respect to the reduction ratio along the transverse and the longitudinal directions

Specimen / R(%)	T O		T 6	
	L	T	L	T
0	9.5	4.1	5.3	2.8
20	-	-	-	-
30	-	-	5.4	3.3
40	-	-	-	-
50	9.4	7.3	4.6	4.0
60	8.5	7.0	4.8	4.7
70	6.4	6.9	-	-
80	7.4	7.6	-	-

Table 4. Variation in fracture elongation (in %) with respect to the reduction ratio along the transverse and the longitudinal directions

Figure 17. a) Variation of the yield strength of T0 tempered composite with respect to reduction ratio

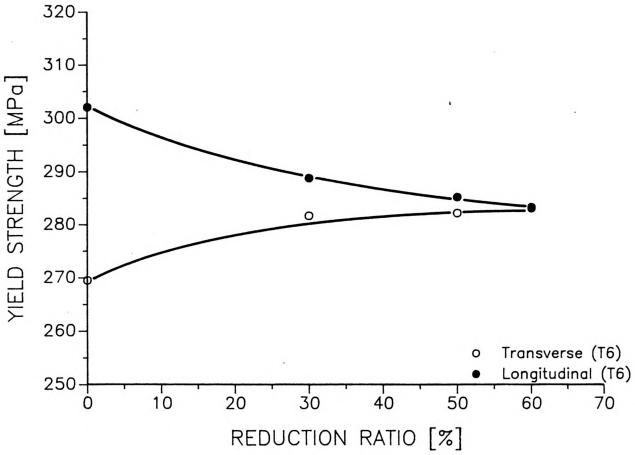
YIELD STRENGTH [MPa]
320
310
300
290
280
270
260
250
0
10
20
30
40
50
60
70
REDUCTION RATIO [%]
Transverse (T6)
Longitudinal (T6)

Figure.17-a)

Figure 17. b) Variation of the yield strength of T6 tempered composite with respect to reduction ratio

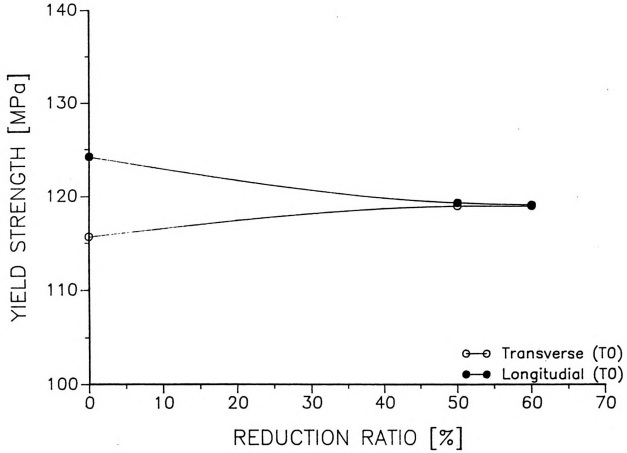
140
130
120
110
100
YIELD STRENGTH [MPa]
0
10
20
30
40
50
60
70
REDUCTION RATIO [%]
Transverse (T0)
Longitudial (T0)

Figure.17-b)

Figure 18. a) Variation of the U.T.S. of T0 tempered composite with respect to reduction ratio

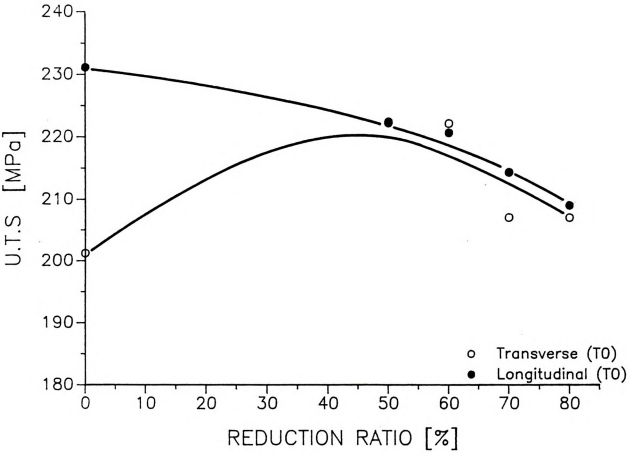
240
230
220
210
200
190
180
U.T.S [MPa]
0
10
20
30
40
50
60
70
80
REDUCTION RATIO [%]
Transverse (T0)
Longitudinal (T0)

Figure.18 a)

Figure 18. b) Variation of the U.T.S. of T6 tempered composite with respect to reduction ratio

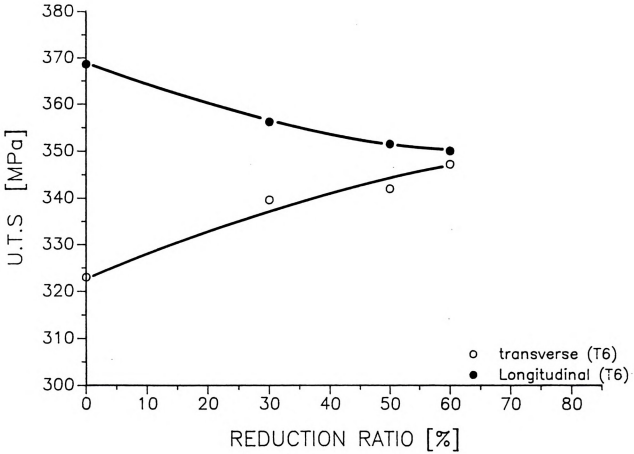
380
370
360
350
340
330
320
310
300
U.T.S [MPa]
0
10
20
30
40
50
60
70
80
REDUCTION RATIO [%]
transverse (T6)
Longitudinal (T6)

Figure.18 b)

Figure 19. Variation of the fracture elongation of T0 and T6 tempered composites with respect to reduction ratio

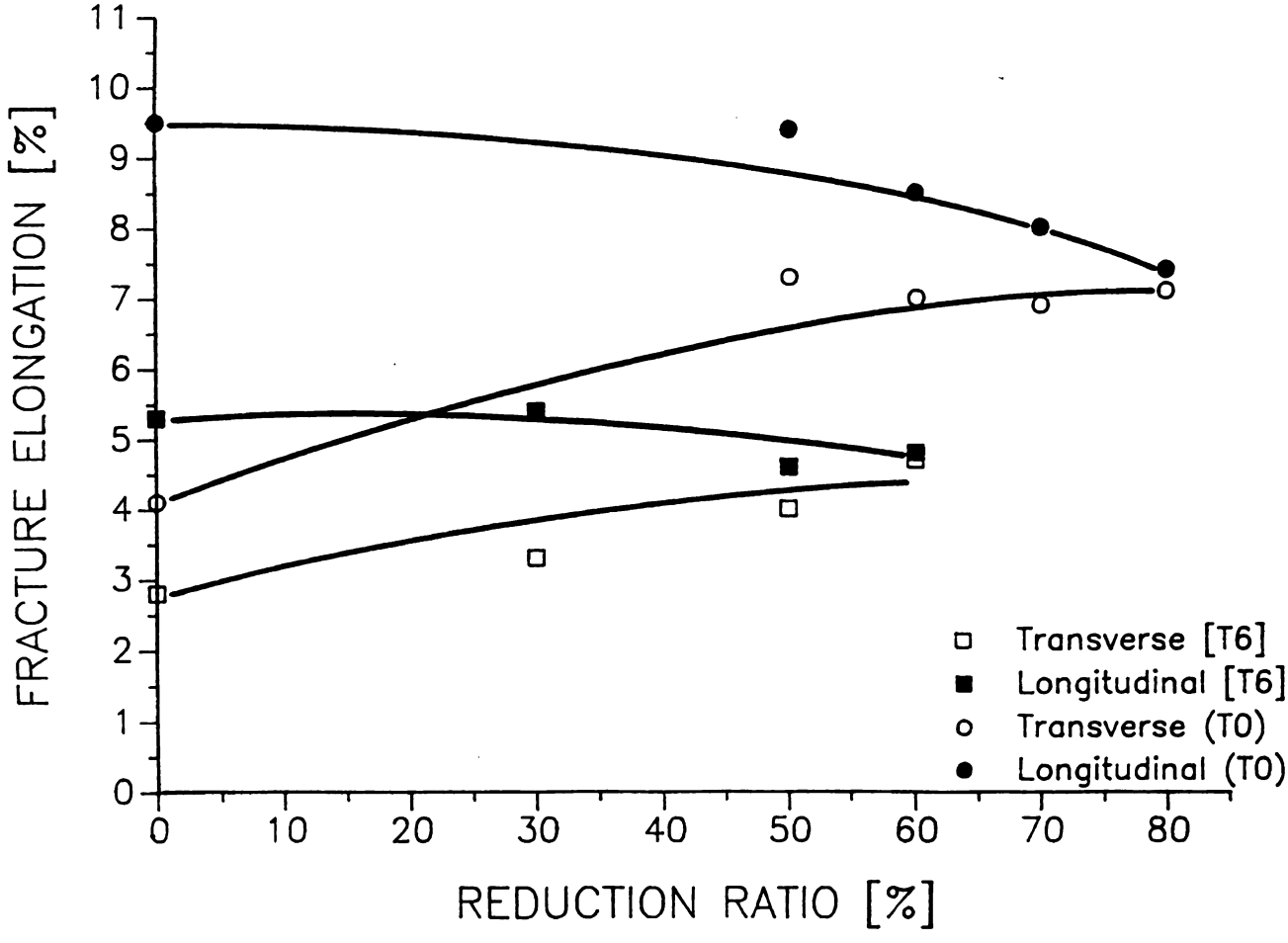
FRACTURE ELONGATION [%]
REDUCTION RATIO [%]
0
1
2
3
4
5
6
7
8
9
10
11
0
10
20
30
40
50
60
70
80
Transverse [T6]
Longitudinal [T6]
Transverse (T0)
Longitudinal (T0)

Figure.19

Figure 20. Optical micrograph illustrating debonded interfaces

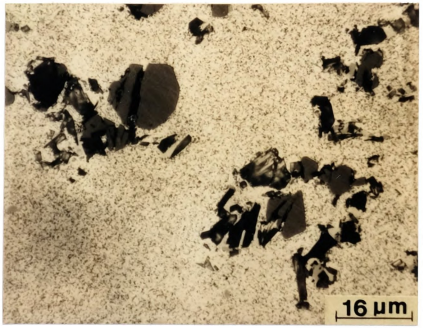

Figure.20

Figure 21. Particulate cracking

a) SEM micrograph
b) optical micrograph.
Note that the matrix is squeezed into the broken particulate in regions indicated by arrow.

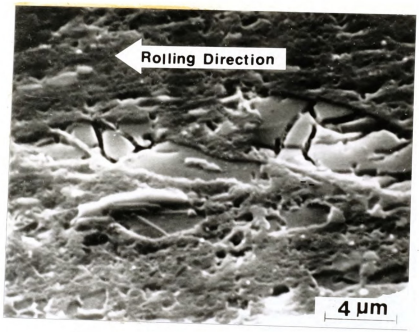

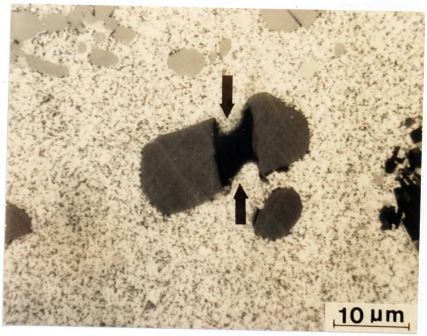

Figure.21

Figure 21. (continued)

c) Particulate cracking in 40 % cold rolled composite
Note the elongated grains in the rolling direction

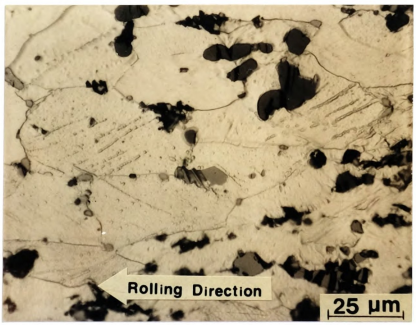

Figure.21 (continued)

Figure 22. Grain size of

a) as-received composite (T6)
b) 30 % warm rolled composite (T6)

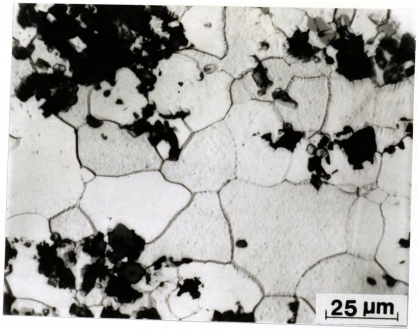

Figure.22

Figure.22. (continued)

c) 70 % warm rollde composite (T6)

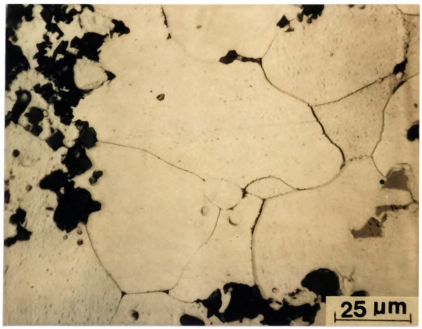

C

Figure.22

Examination of the typical fracture surface of the SiC_p/Al composites, shown in Fig.23), reveals a large amount of localized plastic flow in the matrix surrounding each SiC_p. Particulate pull-out and interface debondings were rarely observed from the fracture surfaces of the tensile specimens. Such a result indicates that the bonding strength between SiC_p and Al matrix is very strong. According to the investigation on the measurement of the interfacial bonding strength of the SiC_p/6061 Al composites, the lower bound value of the interfacial bonding strength for the composites was determined as 1690 MPa [61], which is 30 times higher than the yield strength of T0 treated (fully-annealed) 6061 Al alloy and 7 times higher than the yield strength of T6 treated (artificially aged) 6061 Al alloy.

Some particulate cracking, which is formed perpendicular to the direction of rolling, was observed from the fracture surface of tensile specimen prepared by cutting along longitudinal direction [Fig.24].

On the other hand, the strength and the elongation in the transverse direction were observed to increase after early stage of warm rolling (up to 50 - 60 % of reduction) and decrease afterward.

Both the redistribution of the SiC_p clusters and the formation of the preferential crack initiation sites (such as interface debonding, particulate cracking, and porosity) can be attributed to the changes in the mechanical

Figure 23. Tensile fracture surface exhibiting large amounts of locallized plastic deformation

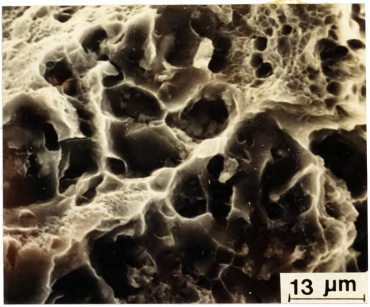

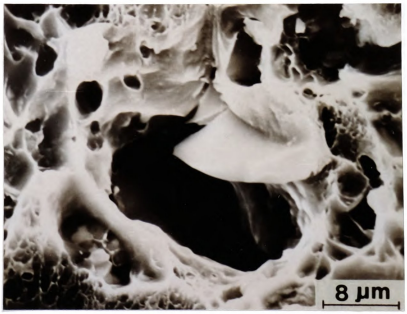

Figure.23

Figure 24. Fracture surface of the longitudinal specimen

Particulate crackings are formed perpendicular to the rolling direction.

Note : "A" particulate has no debonded interface.
"B" particulate has debonded interface which seems to be formed due to rolling.

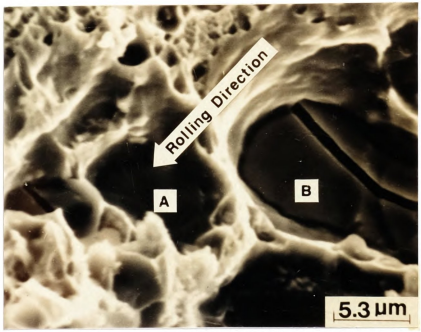

Figure.24

properties in the transverse direction. The redistribution of the SiC_p clusters, which results in more uniform microstructure, appeared to be the main cause for the improvement in the strength and the elongation. But the formation of the preferential crack initiation sites is considered to be the dominant factor for the decrease in such mechanical properties.

4.3 Failure mechanism of the SiC_p/Al composites under uniaxial tension

The failure mechanism of the SiC_p/Al composites under a uniaxial tensile load is analyzed in this section.

From the results of the tensile test, it is clear that the addition of moderate amount of SiC_p (usually less than 30 % by volume) into Al matrix can result in significant increase in the strength, and presumably the elastic modulus, of the composites.

However, the addition of SiC_p into Al-alloy results in substantial decrease in the ductility, and consequently the fracture toughness of the composites, a main drawback for the wide use of most metal matrix composites reinforced with ceramic reinforcements, even at low volume fraction levels.

Recently, several studies have been carried out to improve the ductility and the fracture toughness of ceramic reinforced metal matrix composites. Nevertheless, large differences in the properties of the matrix and reinforcement cause large differences between reinforced and unreinforced alloys. Such big discrepancies in the ductility and the fracture toughness are considered to be a consequence of the unique failure mechanism of the discontinuously reinforced metal matrix composites. Such a behavior is exactly opposite with the failure mechanism of ceramic matrix composites.

However, significant studies have not been carried out so far on the failure mechanism of the SiC_p/Al composite system, or discontinuously reinforced metal matrix compositets.

In 1986, Nutt and Duva [62] have carried out TEM studies on SiC whisker reinforced Al alloy. They observed that the void nucleated at the corner of the whisker ends and grew towards the centers of the whisker ends. They did not obseerved the void formation along the long sides of the whisker/matrix interface, which is parallel to the tensile direction.

From the above experimental results, void nucleation at the SiC_w/Al interface (i.e interface debonding) was proposed as the failure mechanism of the SiC_w/Al composites and as a reason for the low ductility and toughness in such composites [62,63].

In this present experiment, some debonded SiC_p/Al interface was observed at the side-surface of the specimen located just below the tensile fracture surface. Debonded interfaces, which are formed perpendicular to the tensile direction, can be seen in Fig.25). This micrograph was taken at the side-surface of the SiC_p/Al tensile specimen just below the fracture surface. The direction of propagation of void due to debonded SiC_p/Al interface is the same as that of the debonded SiC_w/Al interface observed by Nutt and Duva.

Figure 25. Debonded interface and particulate cracking of tensile fracture surface

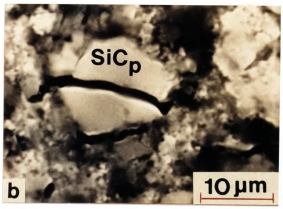

Figure.25

Figure 26. Stress concentration at the pole of the inclusion during uniaxial loading

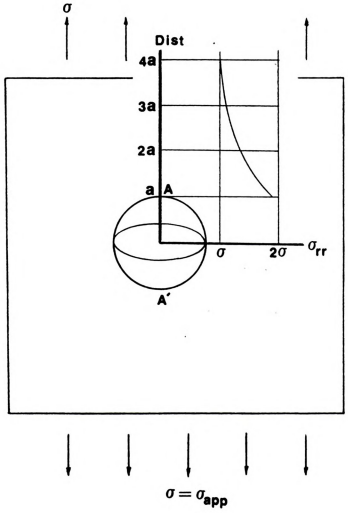

Figure.26

Such a phenomenon of interface debonding can be explained with the help of a simple model of "a rigid spherical inclusion embedded in an elastic solid", shown in Fig.26). If a tensile stress (σ_{app}) is applied on the system, the radial tension (σ_{rr} i.e decohesion stress) at the "pole" of the spherical inclusion (i.e at the point A and A') becomes intensified to a value of

$$\sigma_{rr} = [\ 2/(1+\nu) + 1/(4-5\nu)\ ]\cdot\sigma_{app} \qquad \text{------19)}$$

in the direction of the externally applied tension (σ_{app}) [64]. Substitution of $\nu = 0.33$ for the Al alloy gives

$$\sigma_{rr} = 1.93\cdot\sigma_{app}$$
$$\approx 2\cdot\sigma_{app}$$

in the direction of the applied tensile loading. Such stress concentration (radial tension) at the pole of the rigid inclusion (SiC_p) can attribute to the debonding of the inclusion-matrix interface.

Although the void nucleation mechanism is an evident operating mechanism for the failure of the SiC_p/Al composites, this mechanism seems to be insufficient to explain such a large difference in the ductility between the reinforced and the unreinforced Al-alloy, since the interface debonding due to void nucleation is a very rare event as compared to the cracking of SiC_p. The latter can be observed from the metallographis and fractographis observations provided in Figs.31) and 32).

Another failure mechanism was suggested in 1987 by You et al [65] who conducted an SEM examination on the tensile fracture surface of the SiC_p/Al composites. In you's study, the numbers of the cracked particulates and the debonded interfaces were counted at the fracture surface. From the analysis, the number of the cracked particulate was found to be twice more than the number of the debonded interface.

At the same time, intensive plastic deformation in the matrix between SiC_p was also observed from the side-surface of the tensile specimen located just below the fracture surface. According to the above observation, the matrix failure was proposed as the dominant failure mechanism of the SiC_p/Al composites, i.e the cracking of SiC_p or debonding of SiC_p/Al interface were attributed to the matrix failure.

It is evident from Fig.27) that the crackings of SiC_p always preceed the matrix failure, although severe plastic deformation can be observed in the matrix near the region of particulate cracking. Therefore, the matrix failure mechanism does not seem to be plausible for the failure of the SiC_p/Al composites.

In order to explain why the crackings of the SiC_p preceed the matrix failure, the model of "a spherical inclusion embedded in the elastic material", which is under uniaxial tensile loading , can be introduced again. If an uniaxial tensile load (σ_{app}) is applied on such a composite

Figure 27. Particulate cracking in a tensile specimen

Note : Arrow mark indicates the initiation of crack propagation into matrix.

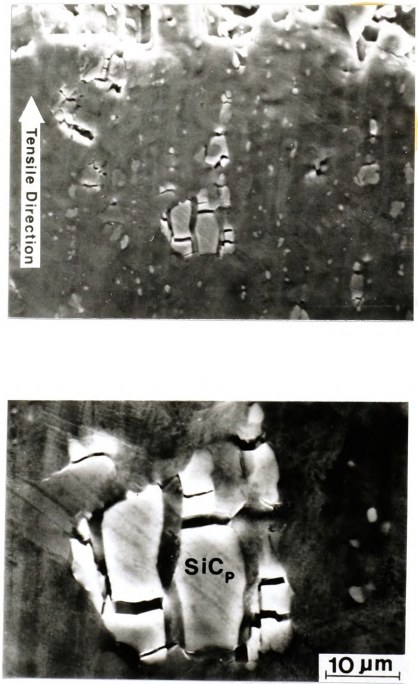

Figure.27

system, the tensile hoop stress ($\sigma_{\theta\theta}$) is induced at the "equator" (i.e BCDB') in the same direction with the applied tension. The stess distribution around the inclusion is shown in Fig.28). The hoop stress ($\sigma_{\theta\theta}$) at the equator is given by Goodier [64].

$$\sigma_{\theta\theta} = [\ (27-15\nu)/(14-10\nu)\ ]\cdot\sigma_{app} \qquad \text{---------20)}$$

Substitution of $\nu = 0.33$ for the Al alloy gives the tensile hoop stress at the equator as

$$\sigma_{\theta\theta} = 2.1\ \sigma_{app}$$

in the direction of the applied tension. However, according to the Saint-Venant's principle, the change in the stress distribution is negligible at a distance larger than the radius of the inclusion (or SiC_p). Therefore, it is evident from Eq.19) and 29) that once the external loal is applied on such a composite system, an inclusion embedded in a matrix acts as a stress raiser.

The Fig.29) shows photoelastic fringes developed around the circular cavity, which enable the visualization of the stress concentration near the cavity. It can be seen that the colored fringes disappear very rapidly as one moves far from the edge of the cavity. This pattern is in good agreement with the Goodier's solution. This indicates that if elastic deformation is assumed for the SiC_p and Al-matrix during the initial stage of tensile loading, the tensile hoop stress near the equatorial surface region of

Figure 28. Stress concentration at the equator of the inclusion during uniaxial tensile loading

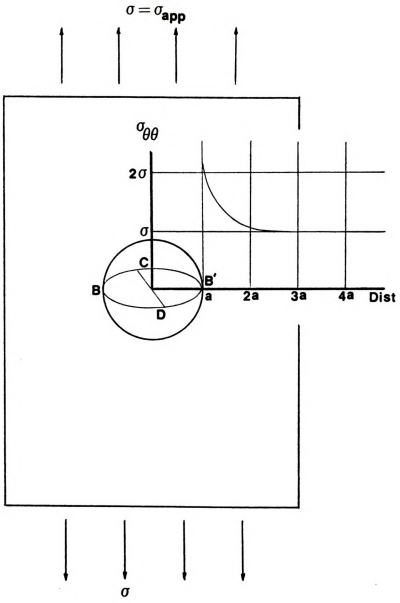
$\sigma = \sigma_{app}$
$\sigma_{\theta\theta}$
2σ
σ
C
B
B'
D
a
2a
3a
4a
Dist
σ

Figure.28

Figure 29. Visualization of the stress concentration near the cavity under uniaxial tension

Note that the stress state in-between the cavities (X) is higher than that of equatorial region indicated by "Y".

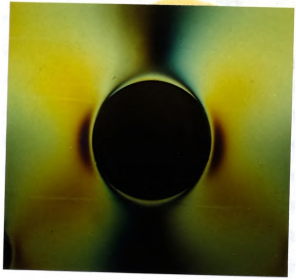

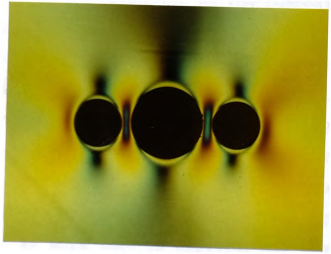

Figure.29

the SiC_p becomes at least twice higher than that of the matrix far from the SiC_p, while the stress in the matrix is the same as the applied tension (σ_{app}). Such stress concentration (tensile hoop stress) at the equator of the SiC_p gives rise to the cracking of the SiC_p. Once the SiC_p has a crack in it, the constraint for the plastic deformation of the Al-matrix will disappear. Then Al-matrix near the SiC_p can now easily undergo plastic deformation causing the opening-up of the cracked planes in the SiC_p as can be seen in Fig.27). This situation can be considered to be same as the Al-alloy which has penny-shaped flaw (or crack) in it. If the external tensile stress is applied further, the penny-shaped crack will propagate into the Al matrix due to the stress concontration at the crack tip. This makes the matrix fail easily and thus the ductility of the composites will decrease substantially.

Based on the present study, the failure mechanism of SiC_p/Al composites can be summarized as follows:

Once a tensile load is applied externally on the composite system, hoop stress and radial stress are generated on the SiC_p in direction of the applied tension. Such stress concentration may cause cracking or interface debonding. As more load is applied, the crack and debonded interface, which are formed already, are easily opened-up due to the plastic deformation of the matrix. New crack will be developed in the matrix at the tip of the opened-up

crack, propagate into matrix, be connected with nearby cracks, and finally form a large void. The whole steps for the failure mechanism is drawn schematically in Fig.30).

The SEM investigation was carried out on the side-surface of the fractured tensile specimen to examine the proposed failure mechanism. Figs.31) and 32) are the micrographs of the side-surface of the tensile specimen located below the fracture surface. Extensive particulate cracking and debonded interface, formed under the applied uniaxial tension, can be seen in this tensile specimen. The cconnection of the near-by cracks into a large crack is illustrated in Fig.31-c). The void formation can be observed in Fig.32-a). Therefore, particulate cracking in addition to interface debonding can be proposed as a major contributor to the failure of SiC_p/Al composites.

Figure 30. The schematic diagram showing the failure mechanism of SiC_p/Al composites under uniaxial tension

a) Generation of tensile hoop stress ($\sigma_{\theta\theta}$) at the equator of SiC_p

b) Formation of crack plane in the SiC_p (Fig.27)

c) Opening-up of crack plane due to plastic flow of Al-matrix (Fig.27)

c') Equivalent diagram of Fig.30-c)

d) Crack propagation inti Al-matrix due to stress concentration build up at the crack tip (Fig.27)

e) Generation of tensile radial stress (σ_{rr}) at the pole of SiC_p

f) Formation of debonded interface

g) Opening-up of debonded interface

g') Equivalent diagram of Fig.30-g)

h) Crack propagation into matrix

i) Joining of cracks (Fig.31-c)

j) Void formation (Fig.32)

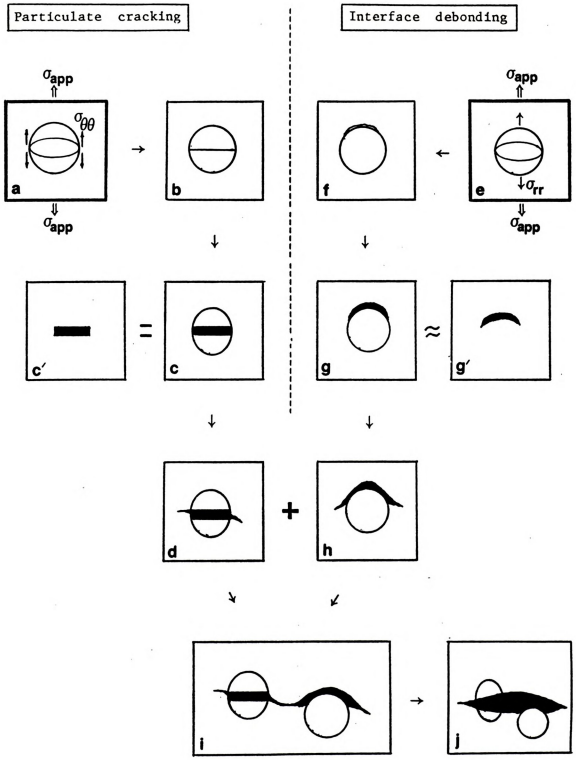
Particulate cracking
Interface debonding
σ_{app}
$\sigma_{\theta\theta}$
σ_{rr}
a
b
c′
c
d
e
f
g
g′
h
i
j

Figure.30

Figure 31. SEM micrograph showing crack development on a tensile specimen (Etched with dilute HCl)

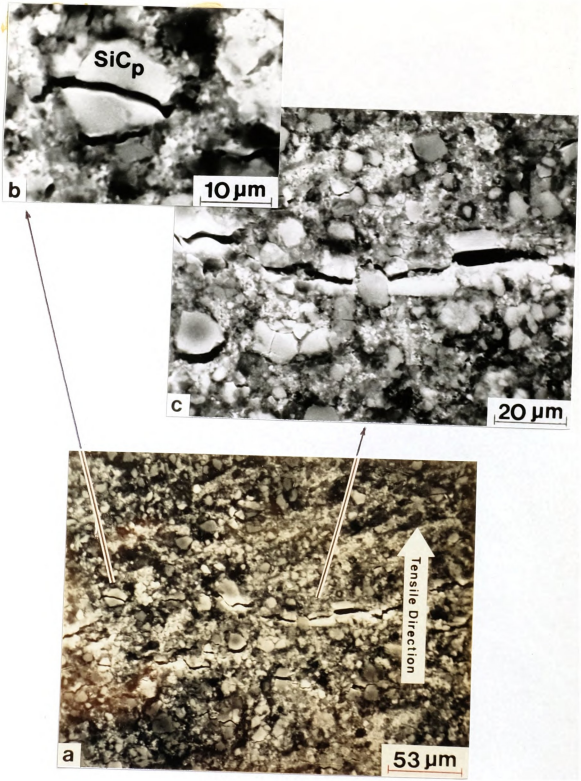

Figure.31

Figure 32. SEM micrograph showing void formation due to joining of cracks (arrow mark)

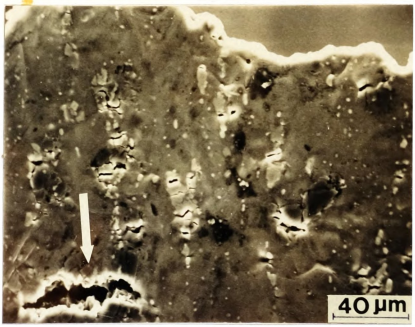

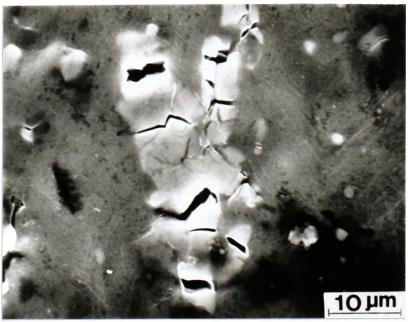

Figure.32

5. CONCLUSIONS

5.1 Strengthening Mechanism of SiC_p/Al composites

1. Some plausible strengthening mechanisms, such as Orowan strengthening, composite strengthening using the modified shear lag theory, thermal strain hardening due to enhanced dislocation density, and strengthening due to subgrain and smaller grain, contribute to the enhanced yield strength of SiC_p/Al composites.

2. Composite strengthening, thermal strain hardening, and strengthening due to subgrain were found to be major contributors to the strengthening of SiC_p/Al composites.

3. On the other hand, it is considered that the effect of the Orowan strengthening is too small as compared to the substantial increase in the yield strength observed in such composites.

5.2 Microstructural Features

1. As-extruded composites (10 % SiC_p/6061-Al) exhibited severely banded structure of SiC_p clusters. Significant redistribution of the SiC_p clusters , which resulted in the uniform distribution of such clusters, was achieved with increasing reduction ratio by both warm and cold rolling. Banded structure of SiC_p clusters totally disappeared beyond 60 % reduction.

2. The cold rolled composites exhibited the presence of larger voids and debonded interfaces as compared to those of the warm rolled composites. Such voids grew larger with increasing reduction ratio.

3. In case of warm rolling, the composites could be rolled down to as much as 85 % of reduction without forming any edge crackings or surface scuffings. On the other hand, in case of cold rolling, edge cracks and surface scuffings were formed before 40 % reduction.

4. Both particulate cracking and interface debonding were observed after rolling; Such features were more predominant in case of cold rolling rather than in warm rolling. There is strong tendency for the crack planes in the particulate to be formed parallel to the direction of rolling pressure, and perpendicular to the rolling direction.

5.3 Mechanical Properties

1. As-extruded composites exhibited anisotropic mechanical properties in their longitudinal and transverse direction. Such anisotropic mechanical properties result from the microstructural inhomogeneity of the as-extruded composites. Mechanical properties become more isotropic with increasing reduction ratio; at about 50-60 % reduction longitudinal and transverse directions possess the same properties

2. Although a significant redistribution of SiC_p clusters was achieved after warm rolling, the principal effect of the warm rolling on the mechanical properties was to decrease the yield and tensile strength as well as the fracture elongation in the longitudinal direction with increasing reduction ratio. However, such properties in the transverse direction were found to increase with increasing reduction ratio up to 60 % and decrease afterwards.

3. The decrease in the mechanical properties in the longitudinal direction can be attributed to the growth of pores, the interface debonding, the particulate cracking, and the grain growth of the matrix during stress relief annealing. On the other hand, the improvement in the mechanical properties in the transverse direction may be due to the redistribution of the SiC_p clusters, which results in more uniform microstructure.

5.4 Failure mechanism of the SiC_p/Al composites under uniaxial tension

1. Interface dedonding due to void formation at the composites interface, which was proposed as a failure mechanism of SiC_w/Al composites by Nutt and Duva, was also observed near the pole of SiC_p. Such an interface debonding is considered to be formed due to the radial tension induced at the pole of SiC_p; the magnitude of this radial tension is almost twice that of the applied tension.

2. The matrix failure mechanism proposed by You et al does not seem to be plausible for the failure of the SiC_p/Al composites, since the crackings of SiC_p were found to always preceed the matrix failure.

3. Tensile hoop stress induced at the equator of SiC_p appears to be responsible for the cracking of SiC_p. The magnitude of the hoop stress was found to be at least twice as large than that in the matrix.

4. Once cracking of SiC_p and debonded interface are formed by the applied tension, such cracks can easily be opened up, connected with each other, and at last make a large void under further applied stress.

5. Particulate cracking under uniaxial tension appears to be a more dominant failure mechanism of the SiC_p/Al composites rather than the void nucleation mechanism at the interface, since the number of cracked SiC_p was observed to be more than that of debonded interface.

6. REFERENCES

1. I.Ahmad, V.P.Greco and J.M.Barranco "Reinforcement of nickel with some high strength filament", J. Composite Materials, 1, 19 (1967)

2. E.G.Wolff "Hydrodynamic Alignment of discontinuous Fibers in a Matrix" Fiber Science and Technology, Elsevier publishing co. Essex. England (1969)

3. N. Tsangarakis, B.O.Andrews and C.Cavallaro "Mechanical properties of some silicon carbide reinforced aluminium composite", J. Composite Materials, 21, 481-492 (1987)

4. T.G.Nieh and D.J.Chellman "Modulus measurements in discontinuous reinforced aluminium composites" Scripta Metallurgica, 18, 925-928 (1984)

5. R.J.Arsenault and S.B.Wu "A comparison of PM vs. melted SiC/Al composites", Scripta Metallurgica, 22, 767-772 (1988)

6. R.J.Arsenault "The strength of aluminium alloy 6061 by fibre and platelet silicon carbide", Material Science and Engineering, 64, 171-181 (1981)

7. Y.Flom and R.J.Arsenault "Interfacial bond strength in an aluminium alloy 6061-SiC composites", J. Metals,38, 31-34 (7.1986)

8. V.C.Nardone "Assessment of models used to predict the strength of discontinuous silicon carbide reinforced aluminium alloys", Scripta Metallurgica, 21, 1313-1318 (1987)

9. R.H.Jones, C.A.Lavender and M.T.Smith "Yield strength -fracture toughness relationship in metal matrix composites", Scripta Metallurgica, 21, 1565-1570 (1987)

10. W.A.Longsdon and P.K.Liaw "Tensile, fracture toughness and fatigue crack growth rate properties of silicon carbide whisker and particulate reinforced aluminium metal matrix composites", Engineering Fracture Mechanics, 24, NO.5, 737-751(1986)

11. T.Christman and S.Suresh "Effects of SiC reinforced and aging treatment on fatigue crack growth in an Al-SiC composites", Material Science and Engineering, 102, 211-216 (1988)

12. J.K.Shang, W.Yu and R.O.Ritchie "Role of silicon carbide particles in fatigue crack growth in SiC particulate reinforced aluminium alloy composites" Material Science and Engineering, 102, 181-192 (1988)

13. H.J.Heine "Cast aluminium metal metrix composites are here", Foundary management & technology, 116, 25-30 (7.1988)

14. F.M.Hosking, F.F.Portillo, R.Wunderlin and R.Mehrabian "Composites of aluminium alloy : fabrication wear behavior", J. Material Science, 17, 477-498 (1982)

15. F.A.Girot,J.M.Quenisset and R.Naslain "Discontinuously reinforced aluminium matrix composites", Composite Science and Technology, 30, 155-184 (1987)

16. V.C. Nardone and J.R. Strife "Analysis of the creep behavior of silicon carbide reinforced 2124 Al (T4)" Metallurgical transaction A, 18A, 109-114 (1987)

17. K.S.Ravichandran "Advanced aerospace Al alloy" J. Metals, 39 28-32 (1987)

18. F.Dolowy "Increasing focus on silicon carbide reinforced aluminium composites", Light Metal Age, 44, 7-14, (6.1986)

19. D.Hughes "Textron unit makes reinforced titanium, aluminium parts", Aviation week and space technology, 129, 91-95, (11.1988)

20. M.A.H.Howes "Ceramic reinforced MMC fabricated by squeeze casting", J. Metals 38, 28-29, (3.1986)

21. F.A.Girot, L.Albingre, J.M.Quenisset and R.Naslain "Rheocasting Al matrix composites", J. Metals, 18-21, (11,1987)

22. T.R.Pritchett "Advenced technology aluminium materials for aerospace application", Light metal age, 44, 10-14 (10.1986)

23. A.Mortensen, J.A.Cornie, and M.C.Flemings "Solidification prossing of metal matrix composites" J. Metals, 12-19 (1988)

24. T.Choh and T.Oki "Wettability of SiC to aluminium and aluminium alloys", The Institute of Metals, 378-385 (1987)

25. V.Laurent,D.Chatain and N.Eustathopoulus "Wettability of SiC to aluminium and Al-Si alloys", J. Material Science, 22, 244-250 (1987)

26. A.Banergi and P.Rohatgi "Cast aluminium alloy containing dispersions of TiO_2 and ZrO_2 particles" J. Material Science, 17, 335-342 (1982)

27. S.Deonath, R.Bhatt and P.Rohatgi "Preparation of cast aluminium alloy - mica particle composites" J. Material Science, 15, 1241-1251 (1980)

28. G.Mott and P.K.Liaw "Correlation of mechanical and ultrasonic properties of Al-SiC metal matrix composites", Metallurgical transaction A, 19A, 2233-2246 (1988)

29. B.C.Pai, S.Pay, K.V.Prabhakar and P.K.Rohatgi "Fabrication of aluminium - alumina (magnesia) particulate composites in foundaries using magnesium addition to the metals", Material Science and Engineering, 24, 31-44 (1976)

30. P.K.Rohatgi, B.C.Pai and S.C.Panda "Preparation of cast aluminium - silica particulate composites", J. Material Science, 14, 2277-2283, (1979)

31. M.K.Surrapa and P.K.Rohatgi "Preparation and properties of cast aluminium - ceramic composites", J. Material Science, 16, 983-993, (1981)

32. T.W.Clyne, M.G.Bader, G.R.Cappleman and P.A.Hubert "The use of δ-alumina fibre for metal matrix composites", J. Material Science, 20, 85-96, (1985)

33. B.P.Krishman, M.K.Surrpa, and P.K.Rohatgi "The UPAL process : a direct method of preparing cast aluminium alloy - graphite particle composites", J. Material Science, 16, 1209-1216, (1981)

34. R.Mehrabin, R.G.Riek,and M.C.Flemings " Metallurgical Transaction, 5, 1899-1905, (1974)

35. T.G.Nieh and R.F.Karlak "Hot-rolled silicon carbide - aluminium composites", J. Material Science Letter, 2, 119-122 (1983)

36. J.R.Picken, T.J.Langan, R.O.England, and M.Liebson "A study of the hot working behavior of SiC - Al alloy composites and their matrix alloys by hot tortion testing", Metallurgical Transaction A, 18A, 303-312 (1987)

37. K.Kannikeswaran and R.Y.Lin "Trace element effects on Al-SiC interface", J. Metals, 39, 17-19 (9.1987)

38. R.J.Arsenault "Interface in metal matrix composites" Scripta Metallurgica, 18, 1131-1134 (1984)

39. T.Iseki, T.Kameda, and T.Murayama "Interfacial reactions between SiC and aluminium during joining" J. Material Science, 19, 1692-1698 (1984)

40. S.G.Fishman "Interface in composites", J. Metals, 38, 26-27 (3.1986)

41. ASM Metals Handbook, 9th ed, 2, "Properties and selection : Nonferrous alloys and pure Metals", 24-42, (1979)

43. CRC Handbook of Materials Science, 2, 378-380, CRC Press Inc. (1975)

43. J.H.Beatty and G.J.Shiflet "Orowan strengthening by MO_2C fibers and needle interphase precipitates in Fe-C-Mo dual-phase steel", Metallurgical Transaction A, 19A, 1677-1620 (1988)

44. P.M.Kelley "The quantitative relationship between microstructure and properties in two-phase alloys" Int. Met. Reviews. 18, 31-36, (1973)

45. H.L.Cox "The elasticity and strength of paper and other fibrous materials", Br. J. Appl. Phys. 3, 72-79,(1952)

46. V.C.Nardone and K.M.Prewo "On the strength of discontinuous silicon carbide reinforced aluminium composites", Scripta Metallurgica 20, 43-48 (1986)

47. R.J.Arsenault and P.H.Fisher "Microstructure of fiber and particulate SiC in 6061 Al composites" Scripta Metallurgica 17, 67-71 (1983)

48. M.Vogelsang, R.J.Arsenault and P.M.Fisher "An in situ HEVM study of dislocation generation at Al/SiC interface in metal matrix composites", Metallurgical Transaction A, 17A, 379-389 (1986)

49. N.Hansen "The effect of grain size and strain on the tensile flow stress of aluminium at room temperature" Acta Metallurgica 25, 863-869, (1977)

50. R.J.Arsenault and N.Shi "Dislocation generation due to difference between the coefficients of thermal expansion", Materials Science and Engineering 81, 175-187 (1986)

51. V.C.Nardone and J.R.Strife "Analysis of the creep behavior of silicon carbide whisker reinforced 2124 Al (T4)", Metallurgical Transaction A, 18A, 109-114 (1987)

52. H.J.MaQueen and J.J.Jonas "Recovery and recrystallization during high temperature deformation" Plastic deformation of materials, Academic press, New York (1975)

53. H.J.MaQueen, W.A.Wong and J.J.Jonas "Deformation of aluminium at high temperature and strain rates" Can. J. Phys. 45, 1225-1235 (1967)

54. W.A.Wood and W.A.Rachinger J. Inst. Metals 76, 237-253 (1949)

55. M.W.Farag, C.M.Sellars and W.J.Tegart, Deformation under hot working conditions, 60-67, Iron steel Inst. London

56. R.T.DeHoff "Problems solving using quantitative stereology", Applied Metallography editted by V.Voort, Van Nostrand Reinhold Co. New York (1986)

57. R.T.DeHoff and F.N.Rhines, Quantitative Micrography, McGraw-Hill, New York (1968)

58. J.Gurland "Observation on the fracture of cementite particles in a spherodized 1.05 % C steel deformed at room temperature", ACTA Metallurgica, 20, 735-741, (1972)

59. J.D.Lubahn "Simultaneous aging and deformation in metals", Trans AIME, 185, 702-708, (1949)

60. R.E.Reed-Hill Physical Metallurgy Principle, 2nd ed, 347-351, D.Van Nostrand Co. New York (1973)

61. Y.Flom and R.J.Arsenault "Interfacial bond strength in an aluminium alloy 6061-SiC composites", Material Science and Engineering, 77, 191-197, (1986)

62. S.R.Nutt and J.M.Duva "A failure mechanism in Al-SiC composites", Scripta Metallurgica, 20, 1055-1058, (1986)

63. S.R.Nutt and A.Needleman "Void nucleation at fiber ends in Al-SiC composites", Scripta Metallurgica, 21, 705-710, (1987)

64. J.N.Goodier "Concentration of stress around spherical and cylindrical inclusions and flows", J. Applied Mechanics, 55, A-39-43, (1933)

65. C.P.You, A.W.Thompson and I.M.Bernstein "Proposed failure mechanism in a discontinuously reinforced aluminium alloy", Scripta Metallurgica, 21, 181-185, (1987)